J Nanopart Res (2018) 20: 150
https://doi.org/10.1007/s11051-018-4250-2

RESEARCH PAPER

A two-site filtration model for silica nanoaggregate mobility in porous media under high salinity conditions

Amir Taghavy · Ijung Kim · Chun Huh · David A. DiCarlo

Received: 9 January 2018 / Accepted: 2 May 2018 / Published online: 30 May 2018

Abstract A variable-viscosity colloid transport simulator is developed to model the mobility behavior of surface-engineered nanosilica aggregates ($nSiO_2$) under high salinity conditions. A two-site (2S) filtration approach was incorporated to account for heterogeneous particle-collector surface interactions. 2S model was then implemented along with the conventional clean bed filtration (CFT) and maximum retention capacity (MRC) particle filtration models to simulate the results of a series of column tests conducted in brine (8% wt. NaCl and 2% wt. $CaCl_2$)-saturated Ottawa sand columns at various pore velocities (7 to 71 m/day). Simulation results reveal the superiority of the MRC and 2S model classes over CFT model with respect to numerical performance criteria; a general decrease of normalized sum of squared residuals (ca. 20–90% reduction) and an enhanced degree of normality of model residuals were detected for 2S and MRC over CFT in all simulated experiments. Based on our findings, conformance with theories underpinning colloid deposition in porous media was the ultimate factor that set 2S and MRC model classes apart in terms of explaining the observed mobility trends. MRC and 2S models were evaluated based on the scaling of the fitted maximum retention capacity parameter with variation of experimental conditions. Two subclasses of 2S that consider a mix of favorable and unfavorable attachment sites with irreversible attachment to favorable sites (with and without physical straining effects) were found most consistent with filtration theory and shadow zone predictions, yielding theoretical conformity indices of 0.6 and higher, the highest among all implemented models. An explanation for such irreversible favorable deposition sites on the surface of silica nanoaggregates might be a partial depletion of stabilizing steric forces that had led to the formation of these aggregates.

Keywords Nanosilica aggregates · Subsurface mobility · High salinity · Filtration modeling · Anocolloids · Oil recovery application

Electronic supplementary material The online version of this article (https://doi.org/10.1007/s11051-018-4250-2) contains supplementary material, which is available to authorized users.

A. Taghavy
Department of Civil and Environmental Engineering, University of Massachusetts Dartmouth, Dartmouth, MA 02747, USA

I. Kim
Department of Civil and Environmental Engineering, Western New England University, Springfield, MA 01119, USA

C. Huh · D. A. DiCarlo (✉)
Department of Petroleum and Geosystems Engineering, The University of Texas at Austin, Austin, TX 78712, USA
e-mail: dicarlo@mail.utexas.edu

Introduction

Surface-engineered silica nanoparticles ($nSiO_2$) have been produced with food-grade quality and used in biotechnology, food-processing, and medical research (Lundqvist et al. 2004; Roy et al. 2005). Organically modified $nSiO_2$ particles have overcome limitations of their unmodified silica counterparts (Roy et al. 2005)

granting them robust amphiphilic properties (Wang et al. 2012) that yield high colloidal stability in suspensions (Espinoza et al. 2010) able to endure elevated temperatures (Aroonsri et al. 2013) and high ionic strength levels (Kim et al. 2015). Hence and more recently, polymer-coated $nSiO_2$ has been extensively researched for utility in subsurface engineering and enhanced oil recovery (Aroonsri et al. 2013; Worthen et al. 2013; Miranda et al. 2012). This includes improving the volumetric sweep efficiency of injected fluids in CO_2-flooding (Yu et al. 2012; Mo et al. 2012) and water-flooding (Ponnapati et al. 2011) applications, mobility control through the spontaneous formation of nanoparticle-stabilized emulsions and foams (DiCarlo et al. 2011; Zhang et al. 2010), wettability alteration (Roustaei et al. 2013; Ju et al. 2002), and interfacial tension reduction (Roustaei et al. 2013).

Effective deployment and delivery of $nSiO_2$ to the target zone within the subsurface will be essential to the successful field-scale implementation of this class of nanoparticle-based technologies. This necessitates an accurate understanding of the mobility behavior of $nSiO_2$ in porous media for development of particle transport models as effective predictive and design tools. Equilibrium adsorption isotherms have served as conventional fate descriptors for solute transport; however, their application to nanoparticles lacks scientific justification (Praetorius et al. 2014; Cornelis 2015). Nanoparticle suspensions are thermodynamically unstable, and their mobility behavior is controlled by kinetic attachment and detachment processes (Petosa et al. 2010) that are described by Derjaguin-Landeau-Verwey-Overbeek (DLVO) theory of colloidal stability (Derjaguin and Landau 1941; Verwey and Overbeek 1948). At high ionic strength levels with suppression of electrostatic repulsion, non-DLVO forces such as steric, hydrophobic, and hydration forces can control particle mobility (Petosa et al. 2010). Macroscopic scale mass transfer of nanoparticles from the fluid phase to solid surfaces is commonly described by advection-dispersion equation (Praetorius et al. 2014; Elimelech et al. 2013), incorporating an additional term to account for surface accumulation of particles on solid phase where the clean-bed filtration theory (CFT) (Yao et al. 1971) or a modified version of it which considers a maximum attainable surface coverage or retention capacity (MRC) (Ko and Elimelech 2000; Li et al. 2008) is commonly adopted. Few recent modeling studies have outlined a need for more complex multi-attachment-site (Zhang et al. 2015, 2016; Park et al. 2016; Sasidharan et al. 2014) or multi-porosity region (Suddaby et al. 2014; Simunek et al. 2013) filtration models for proper core-scale description of the transport and deposition of nanocolloids in porous media. These alternative calls of model approaches include the two site filtration approaches that allows for (i) fast (equilibrium) and slow (kinetic) attachment (Martin and Olusegun 2014; Wei et al. 2017) or (ii) reversible and irreversible attachment to fixed capacity MRC sites (Zhang et al. 2015, 2016) or mixed CFT and MRC types (Fang et al. 2013).

Kim et al. (2015) investigated the effects of flow velocity, particle size, and concentrations on the mobility of $nSiO_2$ aggregates in sand columns saturated with API brine (8% wt. NaCl and 2% wt. $CaCl_2$). In their study, a gradual increase in the efflux of particles with time was observed in all experiments that could not be explained by CFT. Although an MRC approach with rate-limited particle detachment captured the experimental particle breakthrough and elution, the scaling of the fitted attachment efficiency and site blocking parameters with variations in flow velocity, mean particle diameter, and effective viscosity were not consistent with the underpinning colloid filtration theories. This implicated the necessity of further refinement of existing mathematical modeling frameworks for particle filtration in order to have an accurate description of $nSiO_2$ mobility under high salinity conditions. This is especially important in the upscaling process to make large-scale predictions of particle mobility. For instance, foams have been used as an enhanced oil recovery technique with application as hydrocarbon mobilizing agents and/or flood-conformance enhancers (DiCarlo et al. 2011; Baran and Cabrera 2006). In the latter case and specifically for CO_2 in brine foams stabilized by surface-engineered $nSiO_2$, the foam-induced flow redistribution in stratified formations has been demonstrated to be highly sensitive to slight variations in core-scale $nSiO_2$ mobility parameters (Worthen et al. 2015).

In this mathematical modeling study, in order to provide an improved mechanistic description of Kim et al. (2015) observations of aggregated $nSiO_2$ mobility under API brine salinity, we develop a class of two-site attachment filtration models (2S) and evaluate its applicability to simulating pre-aggregated $nSiO_2$ elution data. Inter-model and intra-class comparisons are made between CFT model, MFT model, and four subclasses of 2S model, respectively. Model performances are gauged and analyzed in terms of (i) the goodness of fit criteria

and (ii) consistency of model fits with underlying colloid filtration theories by introducing two theoretical compliance indices to quantify the consistency of the velocity, viscosity, and size dependence of the fitted particle mobility parameters with colloid filtration and shadow zone theories.

Methods

Experiments

Mobility tests, fully described in Kim et al. (2015), were carried out by injecting pre-aggregated $nSiO_2$ dispersions ranging in mean particle size between 5 nm and 2 μm through a 30-cm-long Ottawa sand column (d_{50} = 350 μm). In each experiment prior to injection of nanoaggregates, the sand column was preconditioned with API brine (8% wt. NaCl and 2% wt. $CaCl_2$). The nanoparticle suspension was pumped from a 400-mL floating-piston accumulator to the column at a controlled variable rate of 2.5, 5, or 25 mL/min corresponding to a hydraulic residence time ranging from 2 to 24 min. An approximate 4.5 pore volume wide (PV) pulse of $nSiO_2$ suspension was injected and was followed by another 4.5 PV of particle-free background brine. The influent and effluent samples were analyzed for silica concentration using inductively coupled plasma-optical emission spectrometry (ICP-OES, Varian). The schematic test setup is shown in Fig. 1, and the experimental conditions are summarized in Table 1.

Viscosity measurement (Kim et al. 2015) for $nSiO_2$ suspensions varying in concentration between 0.5 and 2% wt. was taken in steady rate sweep mode between 10 and 1000 s^{-1} shear rate using a rheometer (ARES-LS1, TA Instruments) with the double-wall couette geometry.

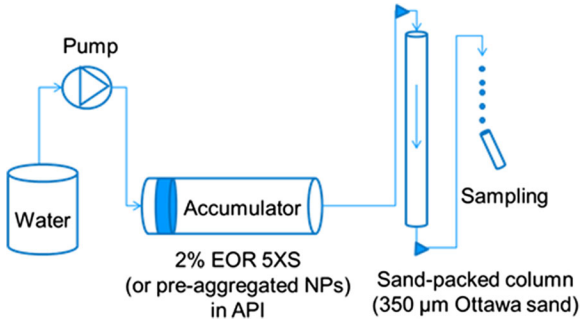

Fig. 1 Schematic view of $nSiO_2$ transport test setup (Kim et al. 2015)

The temperature was controlled by a circulator at 25 °C. Samples of different aggregate sizes were prepared by keeping nanoparticle dispersions exposed to API brine for extended periods of time (at least 48 h). The measured viscosity at 100 s^{-1} of shear rate increased from 1 cP to above 20 cP as $nSiO_2$ concentration increased from 0.5 to 2% wt. in aqueous suspension. The viscosity of $nSiO_2$ suspension was dependent on the $nSiO_2$ concentration under the shear rates tested. The viscosity value corresponding to the shear rate of each mobility test was selected for the simulation.

Mathematical model

Mass balance for particle retention and transport was expressed using 1-D advection-dispersion equation with an additional term for surface mass accumulation on the solid phase to describe $nSiO_2$ mobility in sand columns (Wang et al. 2008):

$$\frac{\partial}{\partial t}(\phi C + \rho_b S) + \frac{\partial}{\partial x}\left[\phi\left(v_w C - D_w^h \frac{\partial C}{\partial x}\right)\right] = 0 \qquad (1)$$

Here x [L] and t [T] denote space and time, C [ML^{-3}] and S [M/M] are the suspended and retained $nSiO_2$ concentrations, ρ_b [ML^{-3}] is the bulk density of the porous medium, v_w [LT^{-1}] and D_w^h [L^2T^{-1}] denote pore velocity and hydrodynamic dispersion coefficient, and ϕ [−] is the effective porosity expressed as a function of retained concentration:

$$\phi = \phi_0 - \frac{\rho_b}{\rho_p} \cdot S \qquad (2)$$

where ϕ_0 [−] is clean-bed porosity, and ρ_p [ML^{-3}] is density of particles (for details of the derivation of Eq. 2 see Supporting Information (SI)—Appendix 0). Changes in effective porosity due to particle retention are generally neglected in dilute particle suspension systems, i.e., milligrams per liter concentrations that was exceeded several orders of magnitude by the range of $nSiO_2$ concentrations used in Kim et al. (2015) (i.e., 20–40 g/L). For this reason, changes in local effective porosity and subsequent effect on spatial distribution of flow velocity and particle attachment kinetics were included in this study.

The second term on the time derivative on the left hand side of Eq. 1 accounts for NP solid-phase interactions (i.e., $nSiO_2$ attachment and detachment). A multisite attachment model, with similarities to the approach

Table 1 Summary of experimental conditions of $nSiO_2$ mobility tests

Property	Symbol	Unit	Exp. no. 1	Exp. no. 2	Exp. no. 3	Exp. no. 4
Pre-aggregated			No	Yes	Yes	Yes
Pore velocity	v_w	m/day	7.1	7.1	14.2	71.0
Influent viscosity	μ_w	cP	0.95	30.6	18.3	6.8
Mean particle diameter[a]	d_p	nm	48	1554	1614	2060
Clean-bed porosity	n_0	–	0.39	0.39	0.38	0.36
Influent concentration	C_0	g/L	20.5	21.6	24.5	39.9

[a] Hydrodynamic diameter measured after 48 h in suspension. See Kim et al. (2015) for detailed information on particle size distributions for non-aggregated (size range of 3–100 nm) and pre-aggregated (size range 200 nm to 5μm) $nSiO_2$ particles

presented in Zhang et al. (2016), was employed that allows for particle deposition in two types of capture sites:

$$\frac{\rho_b}{\phi}\frac{\partial S_{CFT}}{\partial t} = \frac{3}{2}\frac{(1-\phi)v_w}{d_c}\alpha_{CFT}\eta_0 C - \frac{\rho_b}{\phi}k_{d,CFT}S_{CFT} \quad (3a)$$

$$\frac{\rho_b}{\phi}\frac{\partial S_{MRC}}{\partial t} = \frac{3}{2}\frac{(1-\phi)v_w}{d_c}\psi_{MRC}\alpha_{MRC}\eta_0 C - \frac{\rho_b}{\phi}k_{d,MRC}S_{MRC} \quad (3b)$$

$$S = S_{CFT} + S_{MRC} \quad (3c)$$

where S_{CFT} and S_{MRC} $[M/M]$ respectively denote the $nSiO_2$ mass concentration attached to (i) CFT sites following clean-bed filtration (Yao et al. 1971) with attachment efficiency α_{CFT} [−] and (ii) MRC sites with attachment efficiency α_{MRC} [−]. η_0 [–], the single collector contact efficiency, is a measure of the frequency of NP-collector surface collisions and was determined using the semi-empirical correlation by Tufenkji and Elimelech (2004) as a function of physicochemical properties of particles, collector surface and flow phase including factors such as particle and collector sizes and fluid velocity and viscosity. The last term (i.e., effective viscosity) was selected based on Kim et al. viscosity measurements and the shear rate corresponding to constant flow velocity of each experiment. The deposition rate of particles in CFT sites (i.e., the attachment rate constant in clean-bed filtration model $k_{att} = \frac{3}{2}\frac{3}{2}\alpha_{CFT}\eta_0$ (Yao et al. 1971)) is independent of deposition history (i.e., no blocking of CFT capture sites); however, the MRC deposition rate approaches zero with full saturation of MRC sites (Li et al. 2008):

$$\psi_{MRC}(S_{MRC}, x) = \left(1 - \frac{S_{MRC}}{S_{max}}\right)\left(\frac{d_c + x}{d_c}\right)^{-\beta} \quad (4)$$

where ψ_{MRC}[−] is the site-blocking function, and S_{max} $[M/M]$ is the maximum retention capacity parameter. The second term on the right-hand side of Eq. 4 accounts for physical straining effects where a micro-scale blocking of pores may occur as a result of deposition of larger aggregates (Bradford et al. 2004). A β value of 0.432 has been used in several existing reports for modeling straining effects for colloidal particles ranging in a hydrodynamic size in the submicron to micrometer scale. (Bradford et al. 2002, 2004). A β value of zero eliminates the straining effects, reducing the site blocking function to the mathematical form proposed in Ko and Elimelech (2000). The last term on the right-hand side of Eq. 3a and Eq. 3b is a kinetic model for particle reentrainment with a first-order dependence on the concentration of deposited NPs and deposition rate constant $k_d[T^{-1}]$.

Numerical implementation

The transport equation (i.e., Eq. 1) was discretized using a Crank-Nicolson finite difference scheme implementing a sequential time-lag approach to solve Eq. 3a,b,c. Three models were fit to $nSiO_2$ mobility data: the two-parameter CFT model (α_{CFT}, k_{det}) (M1), three-parameter MRC model (α_{MRC}, S_{max}, and k_{det}) (M2), and the 2S model class with a maximum of four model parameters (α_{CFT}, α_{MRC}, S_{max}, and k_{det}) where four subclasses were considered (i) the unbounded 2S (M3), (ii) 2S with favorable irreversible attachment to MRC sites (i.e., $\alpha_{MRC} = 1$ and $k_{d,\,MRC} = 0$) (M4), (iii) 2S with physical straining-based irreversible attachment to MRC sites (i.e., $\beta = 0.432$ and $k_{d,\,MRC} = 0$) (M5), and (iv) 2S with irreversible physical straining under favorable attachment conditions (M6). Note that the latter three subclasses of 2S allow for particle detachment only from the CFT sites consistent with the expected irreversibility of particle deposition in deep primary

energy minima under favorable attachment conditions (Petosa et al. 2010) and previous reports on the irreversibility of physical straining (Bradford et al. 2004, 2007).

The nonlinear least squares method was used in the inverse analyses. Parameter estimation follows a two-stage iterative procedure: (stage 1) the injected pulse portion of effluent data was used to estimate all model parameters except for k_{det} which had a fixed value (starting with an initial guess), and (stage 2) k_{det} parameter was then fitted incorporating tailing part of $nSiO_2$ effluent concentrations (corresponding to chase water phase of mobility experiments) with all other mobility parameters fixed at values estimated in stage 1. Stage 1 was repeated using the updated fixed for k_{det}, and iterations continue until a set tolerance of 1% on k_{det} between two successive iterations was satisfied.

Results and discussion

Table 2 provides the fitted particle mobility parameters for experiments 1–4 based on models M1-M6. The $nSiO_2$ in the non-aggregated state (experiment 1), with a mean particle diameter of 48 nm, was highly mobile behaving almost like a conservative tracer (with a fitted $\alpha_{CFT} = 3.7 \times 10^{-4}$) at a pore velocity of 7.1 m/day (the lowest in this study). The pre-aggregated $nSiO_2$ with a mean aggregate diameter ranging between 1.5 and 2 μm, on the other hand, showed remarkably low mobility, far less than what can be attributed to the effect of gravitational sedimentation alone (Fig. 2). Even though the dramatic increase in the mean particle size was associated with a three orders-of-magnitude magnification of the gravity component of contact efficiency (η_G; Tufenkji and Elimelech 2004) from 1.66×10^{-5} (experiment 1) to 0.0162 (experiment 2), the overall single collector contact efficiency (η_0) decreased due to the dampening of Brownian motions of particles with the size increase (0.0592 (experiment 1) versus 0.0214 (experiment 2)). This corresponded to a significant increase of the CFT fitted particle-collector attachment efficiency (α_{PC}; Tufenkji and Elimelech 2004) from 3.7×10^{-4} (experiment 1) to 0.569 (experiment 2). MRC model fitted α_{PC} increased 13-fold between experiments 1 and

Table 2 List of the fitted model parameters for filtration models considered herein

Model	Exp. no.	α_{PC}^{CFT} –	α_{PC}^{MRC} –	S_{max} (g/kg)	k_d (1/s)	β –
M1—CFT	1	*3.7E−04*			*0*	
	2	*1.053*			*5.3E−05*	
	3	*0.345*			*3.5E−05*	
	4	*0.090*			*7.6E−04*	
M2—MRC	1		*0.104*	*0.70*	*0*	0
	2		*1.317*	*41.10*	*4.1E−05*	0
	3		*0.824*	*13.32*	*1.5E−05*	0
	4		*0.183*	*4.22*	*8.0E−04*	0
M3—2S	2	*0.569*	*0.715*	*13.19*	*9.4E−05*	0
	3	*0.175*	*0.798*	*6.80*	*3.9E−05*	0
	4	*0.088*	*0.094*	*3.84*	*1.1E−02*	0
M4—2S − $\alpha_{PC}^{MRC} = 1$	2	*0.697*	1	*5.31*	*4.0E−05*	0
	3	*0.320*	1	*3.52*	*6.0E−05*	0
	4	*0.071*	1	*1.96*	*1.2E−03*	0
M5—2S-str	2	*0.569*	*7.99*	*16.08*	*9.4E−05*	0.432
	3	*0.179*	*11.51*	*7.28*	*4.3E−05*	0.432
	4	*0.037*	*1.70*	*2.77*	*3.6E−03*	0.432
M6—2S-str − $\alpha_{PC}^{MRC} = 1$	2	*0.996*	1	*0.816*	*5.28E−05*	0.432
	3	*0.473*	1	*0.698*	*3.64E−05*	0.432
	4	*0.083*	1	*0.509*	*8.45E−04*	0.432

Italic entries denotes physical quantities

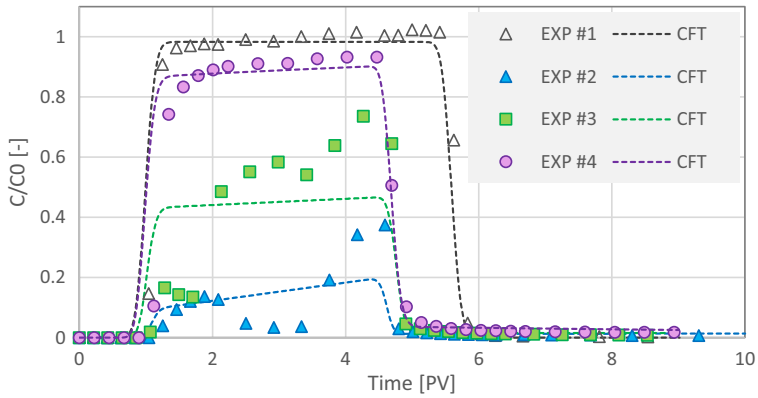

Fig. 2 The experimental $nSiO_2$ effluent concentration and respective best fit by clean-bed filtration (CFT) model

2, suggestive of a lower magnitude of the same trend captured by CFT model. According to classical colloid filtration theory, a change in physical system properties should merely impact η_0-efficiency while α_{PC} is anticipated to be unaffected (Li et al. 2008; Tufenkji and Elimelech 2004). This notable increase of α_{PC}, hence, suggests that the change in particle sizes during the aggregation process reflects not only a change in the physical characteristics of $nSiO_2$ suspension but also a shift in particle surface chemistry. This hypothesis is further corroborated by the presence of persistent tailings of $nSiO_2$ in effluent samples during the post flush with particle-free brine in all experiments with pre-aggregated $nSiO_2$ indicative of reversible attachment as opposed to irreversible attachment observed for non-aggregated $nSiO_2$ in experiment 1 (no tailing on the effluent breakthrough curve was detected during the post flush period in this experiment). Another notable difference in model predictions stemming from the aggregation state of the particles was the computed reduction of the effective porosity of soil (see SI—Appendix B, Table B1), while negligible for non-aggregated $nSiO_2$ (limited to about 0.1%), the effective porosity decreased moderately for pre-aggregated particles (by roughly 0.5–2.5% inversely correlated with flow velocity).

For more in-depth comparison of the implemented modeling approaches, the numerical performance of the CFT and MRC models and four subclasses of 2S model were evaluated through the analysis of (i) modeling residuals (i.e., the difference between modeled and measured effluent concentrations) and (ii) the theoretical conformance of model-specific fitted parameters. The two aspects of model performance assessment are discussed separately hereinafter.

Analysis of model residuals

Comparative analysis of the numerical performance of models M1-M6 was done based on two criteria on the (i) goodness of fit and (ii) distribution of modeling residuals.

Criterion I. Normalized Sum of Squared Residuals (NSSR), as a measure of the goodness of fit, was defined as follows:

$$\mathrm{NSSR}_{i,m} = \frac{\sum_{k=1}^{N_e}\left(C_{m,i}^{k} - C_i^{k}\right)^2}{C_{0,i}^2 \cdot PW_i \cdot (N_i - N_m - 1)} \tag{5}$$

where $\mathrm{NSSR}_{i,\,m}$ [–] denotes the NSSR for experiment i computed based on model m, C_i [ML^{-3}] is a 1-D matrix that stores experimental effluent concentrations, $C_{m,\,i}$ [ML^{-3}] contains the respective modeled effluent concentrations for C_i given by model m, $C_{0,\,i}$ [ML^{-3}] and PW_i [pore volumes] are experiment-specific influent concentration and injected pulse width, and lastly, N_i and N_m denote the numbers of experimental effluent concentration data points and model fitting parameters, respectively. The lower the NSSR value of a model, the better the numerical fit provided by that model. Models with greater number of fitting parameters were penalized following a method similar to calculating adjusted R^2 in multivariate regression (Helland 1987).

Computed NSSRs are shown in Fig. 4. A general improvement in the goodness of fit for MRC and 2S models was observed over the CFT model fits. The unbounded 2S NSSRs were 20–90% lower than CFT-NSSRs in all experiments but remained within a 10% range of MRC-NSSRs with only one exception (experiment 3), implying that the additional intricacies of the

2S class did not help improve model performance with respect to NSSR metric compared to less sophisticated MRC model. The 2S subclass with favorable straining (M6) representation of $nSiO_2$ mobility was notably similar to CFT model in terms of the shape of fitted breakthrough curves (Fig. 3b–d) and calculated NSSR (gray rods vs. hollow blue cones in Fig. 4).

Criterion II. Normality of Model Residuals was characterized for experiments 2–4 by plotting the computed residuals of each model class (i.e., CFT, MRC, and 2S) versus the Gaussian quantiles (referred to as a normal quantile-quantile or Q-Q plot). Models were then compared based on the degree of linearity (R^2 value) of the alignment of model residuals on Q-Q plots (Fig. 5). For a clear visual representation, only the subclass of 2S with favorable attachment to MRC sites (M4) was included in Fig. 5. The MRC (M2) and 2S (M4) models (both implementing three fitting parameters) exhibited generally higher R^2 values than the two-parameter CFT model. All models performed poorly on experiment 4; however, 2S (M4) resulted in a remarkably higher R^2 value compared to MRC model. No consistently discernible improvement to the normality of model residuals was observed for 2S class over MRC, albeit, both model classes showed clear improvement over CFT.

Theoretical conformance of implemented modeling approaches

Comparison of the consistency of the tested filtration models with the underlying theories of colloid deposition in porous media, is outlined in this section. CFT, MRC, and 2S model classes incorporate either one (CFT and MRC) or two (2S) attachment efficiency term(s) (α_{PC}) with the latter two models also implementing a maximum retention capacity parameter (S_{max}). Here we define two indices to quantify the consistency of the scaling of α_{PC} and S_{max} parameters across experiments 2–4.

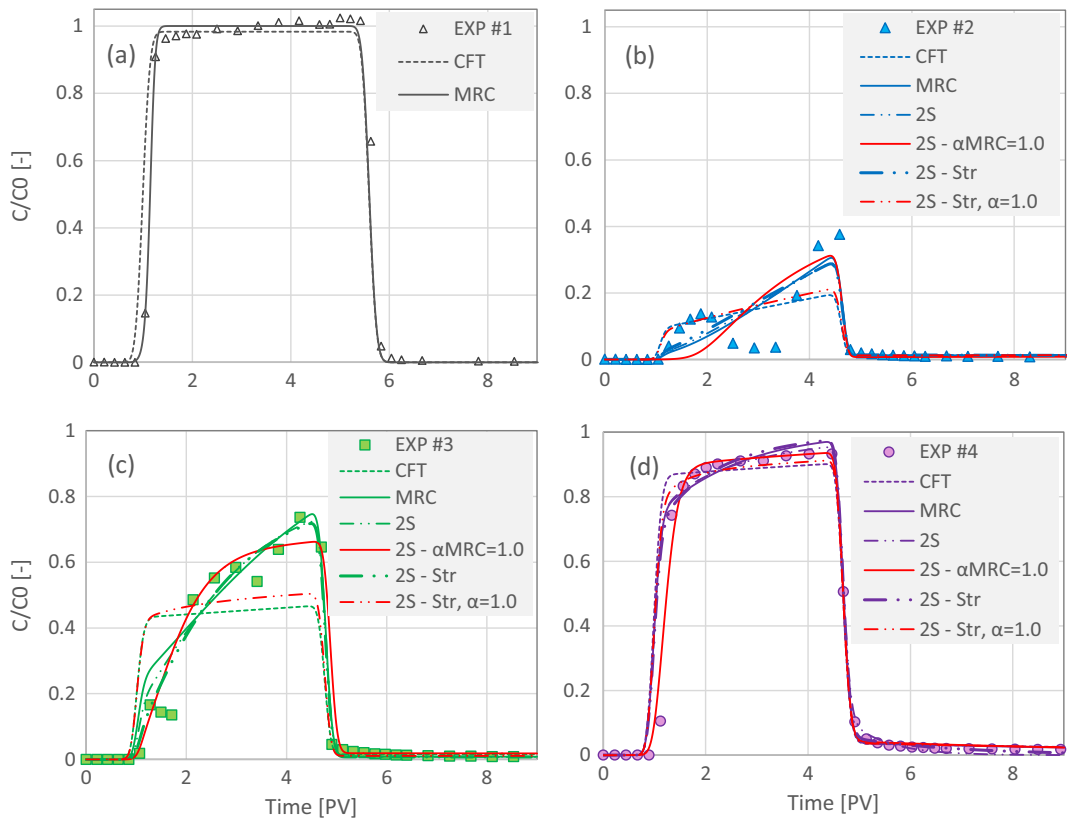

Fig. 3 Best fits provided by CFT, MRC, and 2S class models to $nSiO_2$ effluent data from **a** control non-aggregated (exp no. 1), and experiments conducted using pre-aggregated $nSiO_2$ at fixed interstitial velocity of **b** 7.1 (exp no. 2), **c** 14.2 (exp no. 3), and **d** 71 m/day (exp no. 4)

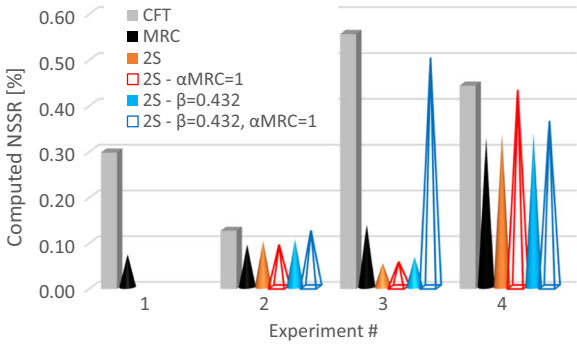

Fig. 4 Normalized squared sum of residuals computed for experiments 1–4 based on different models

A quantitative analysis of the fitted detachment rates was not undertaken. To the best of our knowledge, colloid reentrainment kinetics in the absence of double-layer interactions has not been mechanistically characterized at macro-scale, and the existing literature only qualitatively explains the observed trends in particle detachment by balancing microscopic adhesive and hydrodynamic drag torques acting on deposited particles (Raychoudhury et al. 2012; Bergendahl and Grasso 2000). An increase in pore water velocity is expected to increase the drag torque on particles submerged in a Newtonian fluid. However, the higher shear rate associated with a higher velocity can reduce the drag torque due to a reduction of the effective viscosity caused by shear thinning behavior of $nSiO_2$ suspension in pre-aggregated state. Increasing the interstitial velocity from 7.1 (experiment 2) to 71 m/day (experiment 4) resulted in a 19–30-fold increase of fitted k_d by all models with the exception of the unbounded 2S (M3) with a 2 orders of magnitude increase of k_d. The CFT- and unbounded 2S-fitted detachment rate constant changed very little (< 10%) when pore velocity increased to 14.2 m/day (experiment 3). In comparison, k_d fitted values of MRC and 2S with straining (M5) decreased more than 2-fold. M4 subclass of 2S was the only model that indicated a k_d increase of 1.5-fold. Note that this subclass considered favorable irreversible attachment to MRC sites.

Attachment efficiency scaling Filtration theory predicts that the attachment efficiency, the fraction of particle-collector collisions resulting in sticking, depends solely on the solution and surface chemistry (Tufenkji and Elimelech 2004). This implies an expected insensitivity of the fitted α_{PC} to variations of physical factors such as particle size and flow velocity. That is, the ratio of attachment efficiencies for two mobility experiments conducted under similar chemistry is expected to be close to unity. Therefore, a deviance from unity of this ratio obtained from model *m* fits can be regarded as a measure of inadequacy of that filtration model for capturing the physics of particle mobility behavior under the respective experimental conditions. On this basis, a theoretical deviance index was defined as follows:

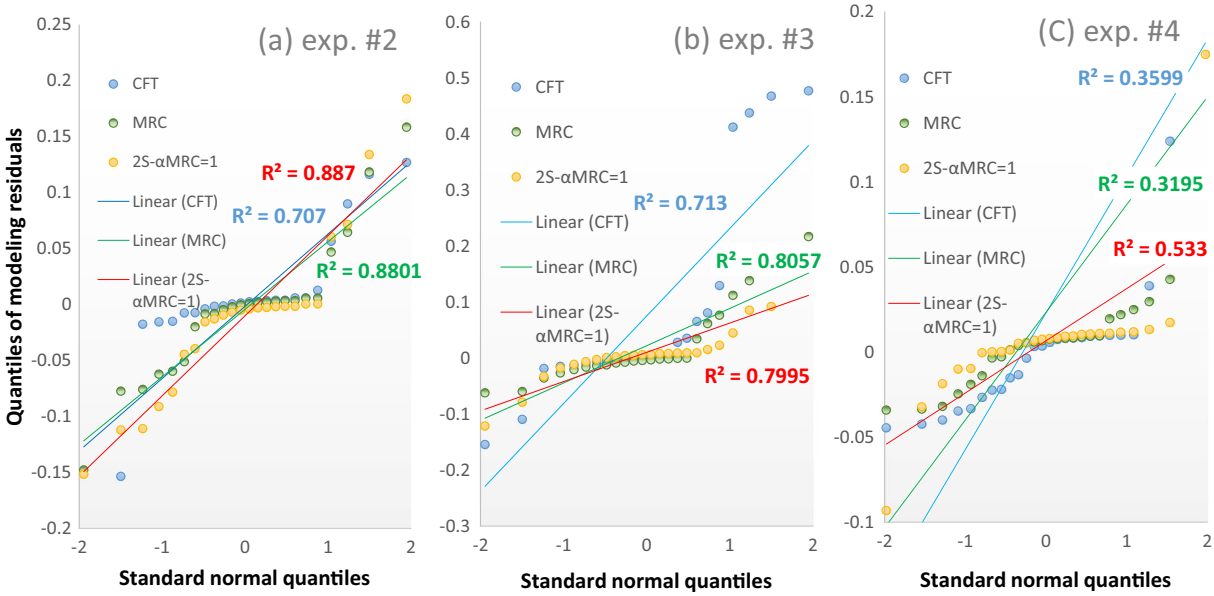

Fig. 5 CFT, MRC, and 2S-α_{MRC} = 1 model residual quantiles plotted versus standard normal quantiles for experiments on pre-aggregated $nSiO_2$ at fixed interstitial velocity of **a** 7.1 (experiment 2), **b** 14.2 (experiment 3), and **c** 71 m/day (experiment 4)

$$TDI_m = \frac{\alpha_{PC}^{m,0}}{\sqrt[N-1]{\prod_{i=1}^{N-1} \alpha_{PC}^{m,i}}} \quad (6)$$

where $\alpha_{PC}^{m,0}$ and $\alpha_{PC}^{m,i}$ are model m fitted attachment efficiencies for experiment i, with superscript "0" denoting the reference experiment with the highest α_{PC} (experiment 2 in this study). Because of similarity in chemical conditions, data from experiments 2–4 were used to determine TDI values. For the 2S class, the geometric mean of α_{PC}^{CFT} and α_{PC}^{MRC} values was used. Figure 6a shows the computed TDIs. CFT model was found most deviant with a TDI value of 4.8 whereas the lowest TDI value of 2.2 was calculated for a subclasses of 2S that considered irreversible favorable attachment to MRC sites (M4 and M6). These subclasses are three-parameter versions of 2S with the same number of fitting parameters as the MRC (M2) model that yielded a notably higher TDI of 3.4. The unbounded 2S (M3) and staining-based 2S (M5) TDIs of 3.1 and 3.2 also exhibited a higher degree of deviance compared to M4 and M6. Care must be taken in the interpretation of staining-based 2S model results (M5 and M6). In the case of unbounded straining (M5), the fitted α_{PC}^{MRC} ranged between 1.7 and 11.5 where an α_{PC} value in excess of one is not theoretically meaningful (Yao et al. 1971; Elimelech and O'Melia 1990). Nevertheless, instances of attachment efficiencies greater than one are not uncommon in colloid filtration literature (Kuhnen et al. 2000; Litton and Olson 1993). Even though the straining model with favorable attachment (M6 with $\alpha_{PC}^{MRC} = 1$) yielded one of the lowest TDI values, it should be noted that M6 performed poorly relative to other 2S subclasses with respect to model residuals.

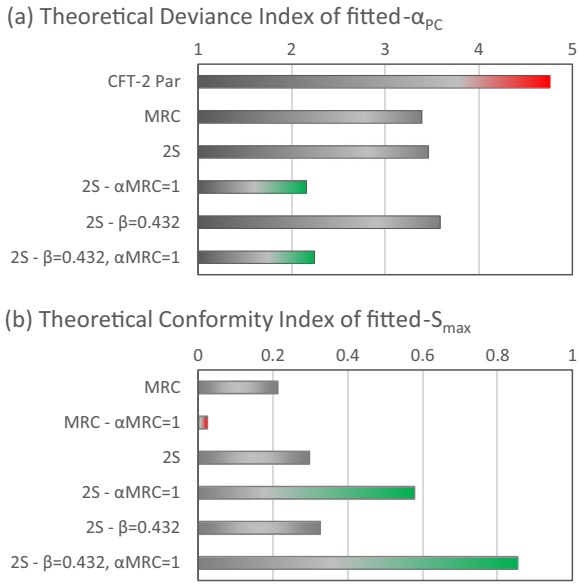

Fig. 6 Model-specific **a** theoretical deviance index (TDI) and **b** theoretical conformity index (TCI) for implemented model classes

Retention capacity scaling The scaling of fitted S_{max} parameter with changes in aggregate size, flow rate, and measured effective viscosity across experiments 2–4 is compared with the predicted S_{max} scaling according to the shadow zone theory (Ko and Elimelech 2000). A shadow zone is thought to be created on the collector surface down gradient of deposited particles, where the probability of subsequent attachment is greatly reduced due to the combined effects of the tangential component of flow around collector grains and double-layer repulsion. Particle size has been shown to be an important factor in the dynamics of particle deposition and blocking in stagnation point flow cell studies (Böhmer et al. 1998). In theory, an increase in the size of particles, fluid viscosity, and/or approach velocity can lead to an increase in the excluded surface area for particle-collector collisions (reduction in maximum attainable surface coverage), which attributed to an enhancement of the shadow effect. Based on this theory, Li et al. (2008) suggested $S_{max} = 19.6\ \Lambda^{-1.2}$ with Λ [–] as a normalized mass flux term approximated by Peclet number as $\Lambda \approx Pe^{1/3} \cdot (d_c/d_M)$ in which d_c [L] and d_M [L] denote the median and a medium sand grain diameter (Li et al. 2008). Peclet number is defined as $Pe = (v_w \cdot d_c)/D_p$ with D_p [L^2T^{-1}] as the particle diffusivity coefficient calculate via Einstein-Stokes equation as follows:

$$D_p = \frac{k_B \cdot T}{3\pi \cdot \mu_w \cdot d_p} \quad (7)$$

where k_B [$J\ K^{-1}$] and T [K] are Boltzmann constant and temperature, respectively. The following theoretical expression can be derived to explain the scaling of S_{max}:

$$S_{max} \propto \frac{1}{\Lambda^{1.2}} \propto \frac{1}{(Pe^{1/3})^{1.2}} \propto \frac{1}{\left((v_p/D_p)^{1/3}\right)^{1.2}} \propto \frac{1}{\left(\left(v_p/\left(\frac{1}{\mu_w} \cdot \frac{1}{d_p}\right)\right)^{1/3}\right)^{1.2}} \quad (8)$$

In other words, if for a given set of μ_w^0, d_p^0, and v_p^0 at a reference state, S_{max}^0 is measured, then, it is expected that S_{max} for μ_w, d_p, and v_p will theoretically follow:

$$S_{max}^{theory}\left(\mu_w, d_p, v_p\right) = \left(\frac{\mu_w^0 \cdot d_p^0 \cdot v_p^0}{\mu_w \cdot d_p \cdot v_p}\right)^{0.4} \cdot S_{max}^0 \qquad (9)$$

Using experiment 2 as the reference experiment and the respective model-specific S_{max} as S_{max}^0, the theoretical S_{max}^{theory} values were derived for experiment 3 and 4 from Eq. 9. The overall consistency of each model with the shadow zone theory predictions was then determined through the computation of a theoretical conformity index (TCI) defined as follows:

$$TCI_m = \sqrt[N-1]{\prod_{i=1}^{N-1} \frac{S_{max}^{i,m}}{S_{max}^{theory}}} \qquad (10)$$

where $S_{max}^{i,m}$ denotes the fitted S_{max} for experiment i by model m, and $N-1=2$ (in this study) is the number of experiments with the exclusion of the reference experiment.

Figure 6b shows the TCIs for MRC and 2S class. The calculated TCIs reveal overall superiority of 2S class compared to MRC class in terms of conformance with shadow zone theory. A TCI value of 0.21 was calculated for MRC (M2) model which was less than respective value for all 2S subclasses (M3-M5). A special one-parameter case of MRC that considered favorable attachment conditions (i.e., $\alpha_{PC}^{MRC} = 1$) produced the lowest TCI (0.02—fits not shown) among all implemented models. Within the 2S class, subclasses with favorable attachment to MRC sites (i.e., M4 and M6) were most conforming with shadow zone theory returning the highest TCIs among the tested models. M4 and M6 returned TCI values of 0.58 and 0.85, respectively, where in comparison, the unbounded 2S (M3) and unbounded 2S with physical straining (M5) yielded a TCI of 0.3 and 0.33.

Conclusions

The transport and retention of pre-aggregated $nSiO_2$ under API brine-saturated conditions were simulated using three classes of colloid filtration models: a clean-bed filtration (CFT) model, a maximum retention capacity (MRC) model, and a two-site mixed type (2S) model. Despite penalizing models for using additional fitting parameters, a general improvement in the goodness of fit (NSSR) was observed for MRC and 2S models over the CFT model. Our findings did not substantiate the adequacy of either of the single-site approaches (i.e., CFT or MRC) to modeling $nSiO_2$ aggregates mobility at high salinity. CFT approach performed poorly with respect to both the goodness of fit and theoretical conformity criteria. This poor performance stems from the inherent incapability of CFT model to explain the gradual increase in particle effluent concentration observed in all pre-aggregated mobility experiments. The reason lies in the assumption of an infinite capacity for attachment to the CFT sites that is independent from the history of colloid retention. Therefore, CFT model cannot explain the observed reduction in the retention capacity of sand columns. CFT model may explain incremental change in particle breakthrough concentrations if the kinetic rate of detachment is comparable to the rate of attachment (same order of magnitude). This explanation, however, is not supported by the low tailing concentrations measured during the post-particle injection chase water flushing period in all experiments. The MRC approach, on the other hand, provided general good fits to mobility data, but the scaling of MRC fitted parameters with variations in physical properties (e.g., velocity and effective viscosity) provided poor theoretical compliance with the physics of colloid filtration and site-blocking.

On the contrary, the 2S class exhibits a superior numerical performance demonstrated by a higher degree of normality of the distribution of model residuals for 2S class compared to CFT model. This superiority was further corroborated by the greater consistency of the 2S class with the underlying principles of colloid filtration in terms of (i) the relative insensitivity of fitted attachment efficiency to changes in system physical properties and (ii) the scaling of fitted retention capacity in accordance with shadow zone theory predictions across a range of experimental conditions. The highest level of conformity with the shadow zone theory and the lowest deviance from filtration theory was yielded by two three-parameter subclasses of 2S (i.e., M4 and M6) that considered irreversible favorable attachment to MRC sites (fixed limited retention capacity) and reversible attachment to CFT sites (infinite capacity) under unfavorable conditions. The 2S subclass with favorable irreversible attachment to MRC subclass (M4) provided (a) one of the closest numerical fits to mobility tests results and (b) the second highest overall theoretical conformity among the tested models. The 2S subclass with favorable straining (M6) yielded the highest overall

theoretical conformance among all tested models suggesting the importance of physical straining as a secondary particle removal mechanism at high salinity, which would be in concert with the larger than colloid straining literature specified critical ratio of 0.002 (Bradford et al. 2004) between mean particle diameter and grain size ratio in pre-aggregated $nSiO_2$ experiments. Both models suggest the existence of favorable attachment sites. A possible explanation is that the same aging or particle surface passivation process that decayed the steric/hydrophobic forces between the interacting particles thereby causing the formation of $nSiO_2$ aggregates might have also created a patch-wise heterogeneity in the distribution of steric forces on the surface of particles colliding collector surfaces. In the absence of electrostatic double layer interactions (due to high salinity), this might have warranted favorable attachment conditions for a fraction of particle-collector collisions. Care must be taken, however, in the interpretation of the results of 2S subclass with favorable straining because of the respective poor fits relative to other 2S subclasses. It must also be noted that numerical fits of the unbounded straining model (M5) were on a par with other subclasses of 2S; albeit, a clear departure from the theoretical principles of filtration was associated with M5 subclass: (i) the significantly larger than unity fitted attachment efficiencies were theoretically inexplicable and (ii) the TDI and TCI indices indicated primitive performance compared to M6 (favorable straining).

Lastly, we should stress the importance of model selection on the upscaling of core-scale particle transport to field-scale mobility predictions, which is culminated in the sensitivity of the estimated effective travel distance to the choice of particle transport model. For instance, for constant velocity fields, CFT model yields the most conservative estimate of particle transport with a distance to three-log removal (a measure of effective travel length (Wang et al. 2008) of $3.07 \times \frac{d_c}{(1-\phi)\cdot\alpha_{PC}\cdot\eta_0}$, an estimation that is independent of the injected mass of particles. On the contrary, the MRC model considers a finite capacity of attachment where distance to three-log removal is a strong function of injected mass of particles. Here upon complete blocking of MRC sites, particles can continue to migrate indefinitely in the subsurface given a sufficient amount of sacrificial particles is injected. 2S model class incorporates a mix of both types, and thus, the upscaled predictions based on 2S class are expected to lie somewhere between the two theoretical extremes depending on the physicochemical characteristics of nanoparticle suspension and site-specific properties of flow and porous media.

Funding information This work was partly supported by the faculty startup fund provided by the College of Engineering of the University of Massachusetts Dartmouth. The authors wish to acknowledge the financial support of Denbury Resources Inc., Plano, Texas.

Compliance with ethical standards

Conflict of interest The authors declare that they have no conflict of interest.

References

Aroonsri A et al (2013) Conditions for generating nanoparticle-stabilized CO2 foams in fracture and matrix flow. SPE annual technical conference and exhibition

Baran JR Jr, Cabrera OJ (2006) Use of surface-modified nanoparticles for oil recovery, U.S. patent no. 7,033,975. Patent and Trademark Office, Washington

Bergendahl J, Grasso D (2000) Prediction of colloid detachment in a model porous media: hydrodynamics. Chem Eng Sci 55(9): 1523–1532

Böhmer MR, van der Zeeuw EA, Koper GJ (1998) Kinetics of particle adsorption in stagnation point flow studied by optical reflectometry. J Colloid Interface Sci 197(2):242–250

Bradford SA, Yates SR, Bettahar M, Simunek J (2002) Physical factors affecting the transport and fate of colloids in saturated porous media. Water Resour Res 38(12). https://doi.org/10.1029/2002WR001340

Bradford SA, Bettahar M, Simunek J, Van Genuchten MT (2004) Straining and attachment of colloids in physically heterogeneous porous media. Vadose Zone J 3(2):384–394

Bradford SA, Torkzaban S, Walker SL (2007) Coupling of physical and chemical mechanisms of colloid straining in saturated porous media. Water Res 41(13):3012–3024

Cornelis G (2015) Fate descriptors for engineered nanoparticles: the good, the bad, and the ugly. Environ Sci: Nano 2(1):19–26

Derjaguin BV, Landau L (1941) Theory of the stability of strongly charged lyophobic sols and of the adhesion of strongly charged particles in solutions of electrolytes. Acta Physicochim URSS 14(6):633–662

DiCarlo DA et al (2011) Mobility control through spontaneous formation of nanoparticle stabilized emulsions. Geophys Res Lett 38(24). https://doi.org/10.1029/2011GL050147

Elimelech M, O'Melia CR (1990) Kinetics of deposition of colloidal particles in porous media. Environ Sci Technol 24(10): 1528–1536

Elimelech M, Gregory J, Jia X (2013) Ch. 6: modelling of aggregation processes. In: Williams RA (ed) Particle deposition & aggregation: measurement, modelling and simulation. Butterworth-Heinemann Ltd, Oxford

Espinoza DA et al (2010) Nanoparticle-stabilized supercritical CO2 foams for potential mobility control applications. s.l., Society of Petroleum Engineers

Fang J, Xu MJ, Wang DJ, Wen B, Han JY (2013) Modeling the transport of TiO2 nanoparticle aggregates in saturated and unsaturated granular media: effects of ionic strength and pH. Water Res 47(3):1399–1408

Helland IS (1987) On the interpretation and use of R2 in regression analysis. Biometrics 43(1):61–69

Ju B et al (2002) A study of wettability and permeability change caused by adsorption of nanometer structured polysilicon on the surface of porous media. s.l., SPE Asia pacific oil and gas conference and exhibition

Kim I, Taghavy A, DiCarlo D, Huh C (2015) Aggregation of silica nanoparticle mobility under high-salinity conditions. J Pet Sci Eng 133:376–383

Ko CH, Elimelech M (2000) The "shadow effect" in colloid transport and deposition dynamics in granular porous media: measurements and mechanisms. Environ Sci Technol 34(17): 3681–3689

Kuhnen F, Barmettler K, Bhattacharjee S, Elimelech M, Kretzschmar R (2000) Transport of iron oxide colloids in packed quartz sand media: monolayer and multilayer deposition. J Colloid Interface Sci 231(1):32–41

Li Y, Wang Y, Pennell K, Abriola L (2008) Investigation of the transport and deposition of fullerene (C60) nanoparticles in quartz sands under varying flow conditions. Environ Sci Technol 42:7174–7180

Litton GM, Olson TM (1993) Colloid deposition rates on silica bed media and artifacts related to collector surface preparation methods. Environ Sci Technol 27(1):185–193

Lundqvist M, Sethson I, Jonsson BH (2004) Protein adsorption onto silica nanoparticles: conformational changes depend on the particles' curvature and the protein stability. Langmuir 20(24):10639–10647

Martin MT, Olusegun AK (2014) Transport of arsenate with iron hydroxide nanoparticles in saturated sand: effects of solution ionic strength, pH, and humic acid. Int J Sci Technol 9(3): 640–654

Miranda CR, Lara LSD, Tonetto BC (2012) Stability and mobility of functionalized silica nanoparticles for enhanced oil recovery applications. s.l., Society of Petroleum Engineers

Mo D, Yu J, Liu N, Lee RL (2012) Study of the effect of different factors on nanoparticle-stablized CO2 foam for mobility control. s.l., Society of Petroleum Engineers

Park CM, Heo J, Her N, Chu KH, Jang M, Yoon Y (2016) Modeling the effects of surfactant, hardness, and natural organic matter on deposition and mobility of silver nanoparticles in saturated porous media. Water Res 103:38–47

Petosa A et al (2010) Aggregation and deposition of engineered nanomaterials in aquatic environments: role of physicochemical interactions. Environ Sci Technol 44(17):6532–6549

Ponnapati R, Karazincir O, Dao E, Ng R, Mohanty KK, Krishnamoorti R (2011) Polymer-functionalized nanoparticles for improving waterflood sweep efficiency: characterization and transport properties. Ind Eng Chem Res 50(23):13030–13036

Praetorius A et al (2014) The road to nowhere: equilibrium partition coefficients for nanoparticles. Environ Sci: Nano 1(4): 317–323

Raychoudhury T, Tufenkji N, Ghoshal S (2012) Aggregation and deposition kinetics of carboxymethyl cellulose-modified zero-valent iron nanoparticles in porous media. Water Res 46(6):1735–1744

Roustaei A, Saffarzadeh S, Mohammadi M (2013) An evaluation of modified silica nanoparticles efficiency in enhancing oil recovery of light and intermediate oil reservoirs. Egypt J Pet 22(3):427–433

Roy I, Ohulchanskyy TY, Bharali DJ, Pudavar HE, Mistretta RA, Kaur N, Prasad PN (2005) Optical tracking of organically modified silica nanoparticles as DNA carriers: a nonviral, nanomedicine approach for gene delivery. Proc Natl Acad Sci U S A 102(2):279–284

Sasidharan S, Torkzaban S, Bradford SA, Dillon PJ, Cook PG (2014) Coupled effects of hydrodynamic and solution chemistry on long-term nanoparticle transport and deposition in saturated porous media. Colloids Surf A Physicochem Eng Asp 457:169–179

Simunek J et al (2013) Numerical modeling of contaminant transport using HYDRUS and its specialized modules. J Ind Inst Sci 93(2):265–284

Suddaby L et al (2014) Experiments and modeling to quantify irreversibility of pesticide sorption-desorption in soil. s.l., American Chemical Society Symposium Series

Tufenkji N, Elimelech M (2004) Deviation from the classical colloid filtration theory in the presence of repulsive DLVO interactions. Langmuir 20(25):10818–10828

Verwey EJW, Overbeek JTG (1948) Stability of lyophobic colloids. Elsevier, Amsterdam

Wang Y, Li Y, Pennell KD (2008) Influence of electrolyte species and concentration on the aggregation and transport of fullerene nanoparticles in quartz sands. Environ Toxicol Chem 27(9):1860–1867

Wang C, Bobba AD, Attinti R, Shen C, Lazouskaya V, Wang LP, Jin Y (2012) Retention and transport of silica nanoparticles in saturated porous media: effect of concentration and particle size. Environ Sci Technol 46(13):7151–7158

Wei H, Yang G, Wang B, Li R, Chen G, Li Z (2017) E. coli interactions, adhesion and transport in alumino-silica clays. Colloids Surf B: Biointerfaces 154:82–88

Worthen AJ, Bagaria HG, Chen Y, Bryant SL, Huh C, Johnston KP (2013) Nanoparticle-stabilized carbon dioxide-in-water foams with fine texture. J Colloid Interface Sci 391:142–151

Worthen A et al (2015) Multi-scale evaluation of nanoparticle-stabilized CO 2-in-water foams: from the benchtop to the field.. s.l., Society of Petroleum Engineers

Yao KM, Habibian MT, O'Melia CR (1971) Water and waste water filtration. Concepts and applications. Environ Sci Technol 5(11):1105–1112

Yu J et al (2012) Foam mobility control for nanoparticle-stabilized supercritical CO2 foam. s.l., Society of Petroleum Engineers

Zhang T, Davidson D, Bryant SL, Huh C (2010) Nanoparticle-stabilized emulsions for applications in enhanced oil recovery. Society of Petroleum Engineers. https://doi.org/10.2118/129885-MS

Zhang T, Murphy MJ, Yu H, Bagaria HG, Yoon KY, Nielson BM, Bielawski CW, Johnston KP, Huh C, Bryant SL (2015) Investigation of nanoparticle adsorption during transport in porous media. SPE J 20(4):667–677

Zhang T, Murphy M, Yu H, Huh C, Bryant SL (2016) Mechanistic model for nanoparticle retention in porous media. Transp Porous Media 115(2):387–406